High-intensity few-cycle laser-pulse generation by the plasma-wakefield self-compression effect

A. Pipahl,[1] E. A. Anashkina,[2] M. Toncian,[1] T. Toncian,[1] S. A. Skobelev,[2]
A. V. Bashinov,[2] A. A. Gonoskov,[2] O. Willi,[1] and A. V. Kim[2]
[1]*Institut für Laser and Plasmaphysik, Heinrich-Heine-Universität Düsseldorf, Universitätsstraße 1, 40225 Düsseldorf, Germany*
[2]*Institute of Applied Physics, Russian Academy of Sciences, 603950 Nizhny Novogorod, Russia*
(Received 24 February 2012; published 18 March 2013)

We present experimental results for laser pulse compression due to wakefield excitation in the relativistic regime using the spectral phase interferometry for direct electric-field reconstruction technique for complete pulse characterization. The results indicate that the pulse was compressed to a 10-fs duration which was verified by fully relativistic three-dimensional particle-in-cell simulations. Optimized modeling based on a hydrodynamic code was also done, showing the possibility of producing laser pulses of few-cycle duration.

DOI: 10.1103/PhysRevE.87.033104 PACS number(s): 52.38.Hb, 42.65.Re, 42.65.Jx

Tremendous progress has recently been made in laser technology primarily based on the chirped-pulse amplification (CPA) [1], allowing ultrashort laser pulse generation with a duration as short as 30 fs and peak power up to 1 petawatt (PW) [2]. Several projects worldwide towards the 10-PW level and higher are now in progress [3]. However, the generation of high power few-cycle pulses, particularly below 10 fs for a Ti:sapphire laser at a wavelength of about 800 nm, is still a formidable task. It is worth noting an alternative to the CPA approach, the Raman amplification scheme [4] which, at the advanced stage, may provide the compression of an amplified seed pulse to a length on the order of a plasma wavelength. The great demand of high intensity few-cycle pulses for various applications ranging from attosecond pulse production [5] to particle acceleration make [6] it challenging for present day laser physics. One of the ways relies on the optical-parametric chirped-pulse amplification (OPCPA) technology [7–9]. However, the progress of this technique in obtaining high energy pulses has been relatively slow. It possesses a high potential, including ultrabroad amplification along with high gain. An alternative way is the recently proposed method for high energy few-cycle pulse generation using the ionization-induced self-compression effect [10], but this method has not been verified experimentally at high energy yet. A plasma-based scheme of pulse self-compression employing the local character of relativistic nonlinearity was analyzed in [11], which has not been realized experimentally either. A very interesting effect is pulse shortening in a plasma wave excited in underdense plasmas. The main features of this effect in the one-dimensional approach were already discussed more than a decade ago [12–14]. However, a key issue that for ultrashort pulses the nonstationary self-focusing effect [15] can strongly influence the dynamical process of pulse self-compression was left unnoticed.

In this paper, we would like to draw the readers' attention to the plasma wakefield self-compression effect for high power ultrashort laser pulses that may be used for few-cycle pulse generation. We first carefully examine the temporal characteristics of the pulses compressed to 10 fs duration by using the spectral phase interferometry for direct electric-field reconstruction (SPIDER) technique after passing a 100-TW, 30-fs pulse through a 2-mm gas jet. These experimental data will be directly compared to three-dimensional (3D) particle-in-cell (PIC) modeling showing that the self-compression of the driver pulse takes place along with the self-focusing effect and is actually based on plasma wave excitation. Then we develop a simplified 3D hydrodynamic model based on a quasi-one-dimensional description of the plasma waves, which agrees qualitatively well with PIC modeling and experiments as well, and use it for optimization with respect to few-cycle pulse generation.

It should be noted that the previous experiments in the relativistic regime [16,17] have confirmed the general predictions for pulse shortening in a plasma wave excited by a pulse. However, going one step further towards few-cycle duration we employed a SPIDER technique for complete pulse characterization, which is proven to be a perfect characterization method for the 10-fs temporal range [18].

The experiment was conducted with the table-top Ti:Sa laser system (ARCTURUS facility; 100 TW, 30 fs, 800 nm, 10 Hz). The linearly polarized laser pulse with an energy of 1.8 J was focused by an $f/7$ off-axis parabola onto a helium gas jet to a focal spot with a diameter of about 10 μm that led to an intensity of 3.4×10^{19} Wcm^{-2} in a vacuum, corresponding to a normalized vector with an amplitude of $a_0 = 4$. The gas jet length is about 2 mm. We have performed the experiments by making a parametric scan in which the plasma densities varied in the range of $n_e = (3\text{–}15)\times 10^{18}$ cm^{-3} obtained by changing the gas pressure.

The transmitted pulse was measured by collimating the central part of the laser beam. Figures 1(a) through 1(d) show the experimentally measured SPIDER interferograms, retrieved (red curves with circles) and approximated by fifth-order polynomials (dashed curves) spectral phase, in Figs. 1(e) to 1(h) the retrieved spectrograms with pulse spectra (on the right side) are shown, and in Figs. 1(i) to 1(l) retrieved pulse intensity profiles for four sequentially increasing electron densities of 8.6×10^{18} cm^{-3} [Figs. 1(a), 1(e), and 1(i)], 1.1×10^{19}cm^{-3} [Figs. 1(b), 1(f), and 1(j)], 1.2×10^{19} cm^{-3} [Figs. 1(c), 1(g), and 1(k)], and 1.5×10^{19} cm^{-3} [Figs. 1(d), 1(h), and 1(l)]. We retrieved pulse shapes [Figs. 1(i) to 1(l)] assuming the spectra to be interferogram envelopes and using the spectral phase approximation by the fifth-order polynomials. After that the spectrograms are obtained [see Figs. 1(e) to 1(h)] for reconstructed pulses defined as

$$S(\omega, T) = \left| \int_{-\infty}^{\infty} E(t) w(t - T) e^{-i\omega t} dt \right|^2, \qquad (1)$$

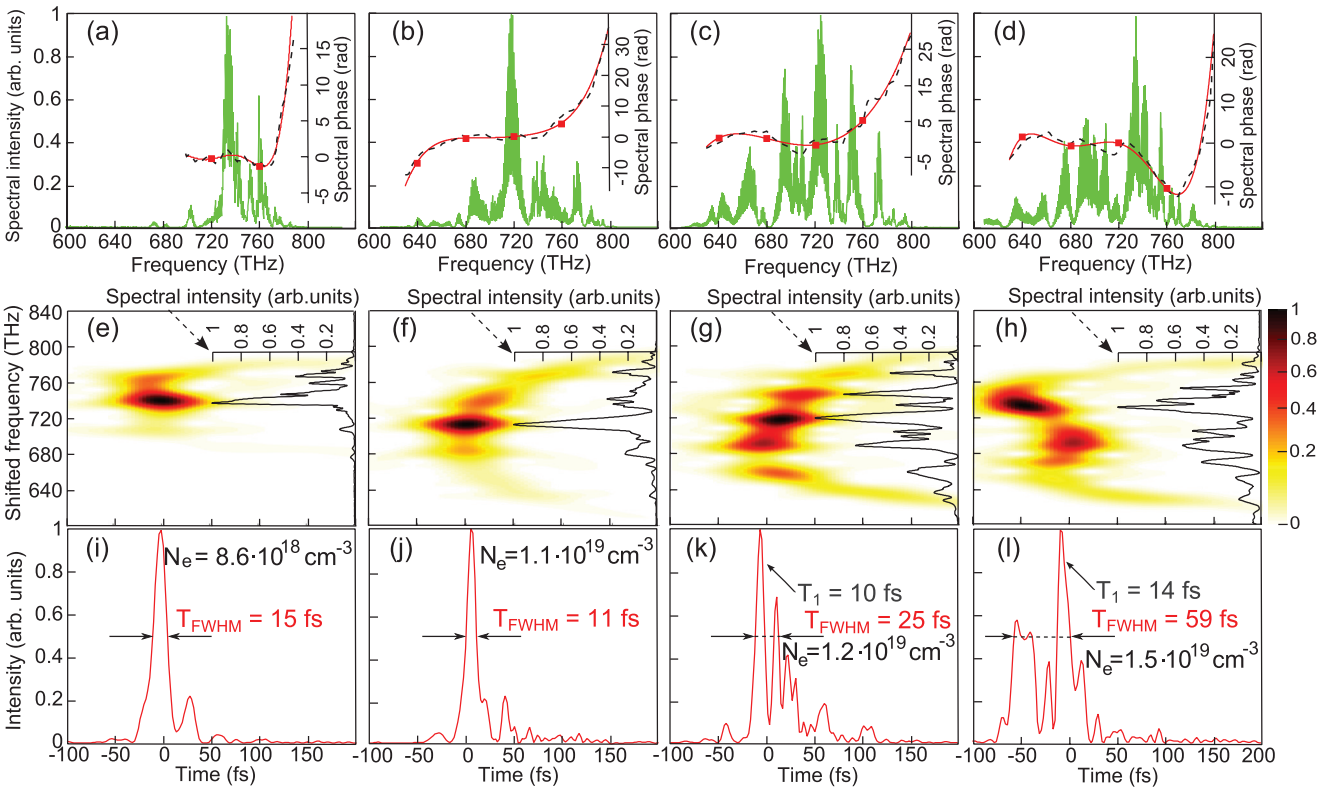

FIG. 1. (Color online) (a)–(d) Experimental SPIDER interferograms [(green) solid curves] for the electron densities of 8.6×10^{18}, 1.1×10^{19}, 1.2×10^{19}, and 1.5×10^{19} cm^{-3}, respectively. The dashed curves are retrieved spectral phases and the (red) curves with circles are their approximation by fifth-order polynomials. (e)–(h) Spectrograms, pulse spectra (on the right side of the box), and (i)–(l) retrieved pulse intensity profiles for the corresponding electron densities.

where $E(t)$ is the laser field and $w(t) = \exp[-t^2/(40\,\mathrm{fs})^2]$ is the window function. The spectrograms display time-dependent spectra: The Fourier transformation is applied to different temporal sections of the signal. They clearly demonstrate how spectral peaks are arranged in the time domain. It should also be noted that the SPIDER application can become challenging when the spectrum is highly modulated or ultrabroadband [19]. Indeed, for fringe structures of the SPIDER interferogram as in the case of Fig. 1, there is an uncertainty for phase retrieval in the frequency regions where the spectral intensities are close to zero. However, by applying a direct pulse reconstruction algorithm, we manually corrected the phase difference by adding or subtracting 2π at the corresponding frequency points, assuming that the intensity laser profile as a whole should be well localized within the subpicosecond time domain.

Let us first pay attention to the low density case of Figs. 1(a), 1(e), and 1(i) and Figs. 1(b), 1(f), and 1(j), where the corresponding plasma wavelengths $\lambda_p = 2\pi c/\omega_p = 11.4$ and 10.1 μm [$\omega_p = (4\pi e^2 n_e/m)^{1/2}$ is the plasma frequency] exceed the pulse length $c\tau = 9$ μm. After the pulse has propagated about 2 mm, the retrieved output pulse durations are about 15 and 11 fs, respectively, i.e., the compression factor increases with the plasma density from 2 to 3 (the initial pulse duration is 30 fs). Therefore, to further increase the compression factor and get sub-10-fs pulses we can use higher plasma densities, which is consistent with the point of view that the interaction efficiency length is inversely proportional to the plasma density. Second, indeed, in the higher density case of Figs. 1(c), 1(g), and 1(k) and Figs. 1(d), 1(h), and 1(l), the pulse spectrum becomes broader, which corresponds to a transform-limited pulse duration of about 5 fs, but the retrieved experimental output pulses are wider and consist of several subpulses of about 10-fs durations. It is important to note that the temporal resolution of the SPIDER technique we used was about 10 fs. We assume that the origin of such subpulse generation is the modulational instability of relativistically intense laser pulses [20]. Summarizing the obtained results we can propose the following scenario of the interaction: During the propagation in the plasma the laser pulse is continuously compressed along with the self-focusing effect shrinking the beam as a whole in the transverse dimensions. However, there is an optimal compression length, where the laser pulse has minimal duration. At higher plasma densities we can assume that either the optimal compression length is less than the plasma width, i.e., 2 mm, or the Raman instability destroys the pulse compression for the input pulse length comparable to the plasma wavelength, which is 9.6 or 8.7 μm for the respective cases.

To properly verify these results and optimize few-cycle pulse generation we employ two numerical codes. The first one is a 3D PIC code, which requires quite essential supercomputer resources for the parameters relevant to the experiment, and the second, more simplified code is based on the hydrodynamic

approach. Here we should mention the new approach for PIC modeling based on boosted frame [21] that could decrease requirements on supercomputer resources.

The fully relativistic PIC code accounts exactly for electromagnetic dispersion as it uses a fast Fourier transformation for field calculations and allows in some cases even a fairly quantitative comparison with the experimental data. The simulation box comoving with the speed of light is $125\,\lambda \times 125\,\lambda \times 100\,\lambda$ and contains $512 \times 512 \times 1024$ cells. Each cell is filled with eight quasiparticles. A linearly polarized laser pulse with a Gaussian envelope $a = a_0 \exp[-(x^2 + y^2)/b^2]\exp[-t^2/\tau^2]$ in both the transverse (x, y) and longitudinal (z) directions is focused normally onto the front edge of the plasma slab from the left side ($z = 0$). Since in the experiment the length of the gas jet was comparable with the beam Rayleigh length, we set the following parameters: $a_0 = 4$, $b = 20\ \mu$m, $\tau = 30$ fs, and a uniform helium plasma slab 2 mm in length, to mimic the experiment. The initial temperature of the electrons and protons is 20 keV. Indeed, at lower densities PIC modeling shows a good agreement with the experimental data, demonstrating continuous pulse compression by a factor of 2 to 3 during the propagation in the plasma. However, at higher densities, the situation is a bit different. It is reminiscent of the previous one only at the initial stage of the propagation, but then the pulse becomes structured, actually consisting of several subpulses. The typical simulation result for a plasma density of 1.3×10^{19} cm^{-3} is shown in Fig. 2. At the beginning, the laser pulse entered into the plasma is continuously shortened during its propagation, sequentially reaching 11.1 fs at a distance of 1.2 mm [Fig. 2(b), blue dashed-dotted line] and then 6.1 fs at 1.28 mm [Fig. 2(b), red solid line]. The most important feature of the compression is that it occurs so that the plasma wave is excited in a quasi-one-dimensional manner, i.e., unlike in the blowout or bubble regime [22]. This is very consistent with the weakly relativistic theory [15] and ensures that the electron density immediately behind the laser pulse is controlled. Indeed, at the beginning of the pulse propagation, the maximum excited plasma wave density is about $0.5n_c$, which is consistent with the one-dimensional (1D) excitation in the relativistic regime. However, during propagation it decreases but is not less than $0.23n_c$, i.e., the electrons under the action of the ponderomotive force do not go around the laser pulse as in the bubble regime but mostly pass through it. Nevertheless, 3D effects are very important for the laser field; we see that the pulse compression is accompanied by relativistic self-focusing where the laser beam diameter shrinks from 20 to 6.5 μm and the output intensity increases up to 10^{20} Wcm^{-2}. Then, at a distance of 1.642 mm, the pulse becomes broader (about 8.5 fs) and structured [Fig. 2(b), violet solid line with triangles], both of these factors increasing with further propagation. Thus, comparing this simulation with the experiment shown in Figs. 1(c) and 1(d) we can conclude that the pulse compression occurs at shorter distances of about 1 mm. The ultrabroad pulse spectrum [Fig. 2(a)] actually reflects the possibility of such compression.

To make careful optimization with respect to few-cycle generation we have developed a simplified hydrodynamic code together with the well-proven slowly evolving wave approach (SEWA) [23]. As the plasma density n_e is much less than the critical value $n_c = m\omega^2/(4\pi e^2)$ ($n_e \ll n_c$) (ω is

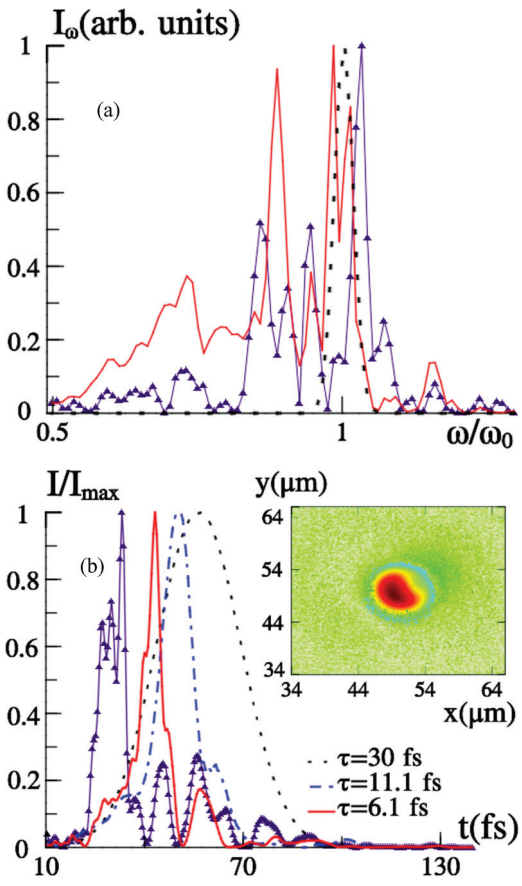

FIG. 2. (Color online) (a), (b) The result of modeling for a 2-mm long plasma with a density of 1.3×10^{19} cm^{-3}: input (dotted line), in the middle $z = 1.28$ mm [(red) solid line] and at $z = 1.642$ mm [(violet) solid line with triangles) pulse spectra, and the corresponding pulse profiles: (blue) dashed-dotted line at $z = 628\ \mu$m, respectively. In the insets: The beam profiles of (b) 6.5 μm in diameter (FWHM) at $z = 1.28$ mm.

the pulse carrier frequency), assuming that the field changes only slightly on the wavelength scale and the transverse size of the beam is large compared to the characteristic longitudinal scale of the field (quasi-optical beam), the Maxwell equations and plasma hydrodynamic equations can be reduced to the following set of self-consistent equations in the corresponding reference frame $\tau = t - z/c$

$$\frac{2}{c}\frac{\partial^2 \mathbf{a}}{\partial z \partial \tau} - \Delta_\perp \mathbf{a} + \frac{\omega_p^2}{c^2}\frac{\mathbf{a}}{1+\Phi} = 0, \tag{2}$$

$$\frac{\partial^2 \Phi}{\partial \tau^2} + \omega_p^2 \frac{(1+\Phi)^2 - (1+|\mathbf{a}|^2)}{2(1+\Phi)^2} = 0, \tag{3}$$

where $\omega_p = (4\pi e^2 n_e/m)^{1/2}$ is the plasma frequency, c is the speed of light in a vacuum, and $\Delta_\perp = \partial^2/\partial r^2 + (1/r)\partial/\partial r$. Here, we introduced the following dimensionless vector and scalar potentials: $\mathbf{a} = e\mathbf{A}/mc^2$, $\Phi = e\varphi/mc^2$. Equation (3) is an ordinary equation of state for a plasma wave [15,24], when the electrons evolve mainly in the longitudinal direction (see also [25]).

A comparison of the results of hydrodynamic modeling with the PIC simulations and experiment shows that they

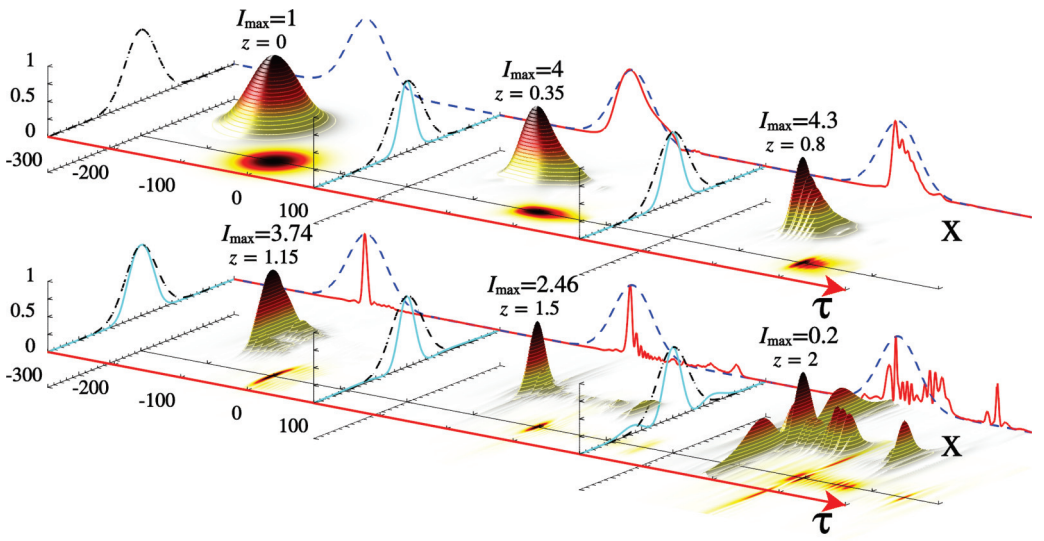

FIG. 3. (Color online) Spatial-temporal pulse dynamics along the propagation direction at a plasma density of 1.3×10^{19} cm^{-3}; additional input (dashed curve) and current [(red) solid line] laser pulse profiles on the axis, and transverse [(blue) solid curve] beam profiles on the plane of maximum intensity are depicted.

are in good agreement. Since we can now follow the propagation dynamics in detail, the peculiarity is that few-cycle pulses are really produced, particularly, for the density of $n_e = 1.3 \times 10^{19}$ cm^{-3}, as in Fig. 2, and $a_0 = 3$ the minimum pulse duration is 1.2 optical periods, i.e., 4 fs, at a distance of 1.15 mm only. But after this point, e.g., at a distance of 2 mm, the pulse splits into subpulses, as can be clearly seen in Fig. 3. It is worth noting that the self-focusing effect is very important, actually exponentially increasing intensity like in [15] and correspondingly accelerating the process of pulse shortening. In Fig. 4 we also show the experimental dependence of the pulse duration (as in Fig. 1) versus plasma density together with the corresponding results of optimization. The optimal intensities for wakefield pulse compression lie in the interval $a \simeq 1$–3, but to obtain the shortest pulse duration

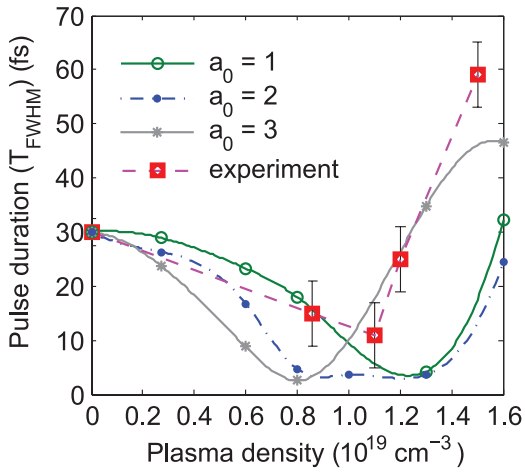

FIG. 4. (Color online) Pulse duration at full-width-half-maximum (FWHM) vs plasma density for a 30-fs laser pulse after 2 mm long propagation: experimental results as in Fig. 1 (red-dashed) and optimized modeling for different incident intensities.

together with the high energy efficiency the plasma density should be matched with the input pulse length, i.e., the pulse length should be comparable to the plasma wavelength. As is seen from Fig. 4, for the plasma length of 2 mm and the input pulse duration of 30 fs, the optimal plasma density is about (0.8–1.2) $\times 10^{19}$ cm^{-3} depending on the field intensity. For example, for $a = 2$ in a quite broad density range around 10^{19} cm^{-3} (dashed-dotted blue curve) a single-cycle pulse of 3.6 fs with an energy efficiency of about 20% is obtained.

In conclusion, we have examined wakefield pulse compression in a combined experimental and numerical study. It is shown that in the relativistic regime ($a_0 \sim 1$–4) laser pulses can be effectively compressed to a duration of few cycles. Moreover, the scheme, as is seen from Eqs. (2) and (3), is scalable to the petawatt level, which means that for present day conventional laser systems delivering comparatively long pulses the wakefield compression opens up a new way of producing PW-class few-cycle pulses. It is also interesting to note that in the alternative to the CPA approach in the advanced stage of the Raman amplification when the amplified seed pulse is compressed to a length on the order of a plasma wavelength, the stage for the wakefield compression can be further applied to obtain very high power few-cycle pulses. It can be applied as an additional final stage of the Raman compression technique or even by properly choosing the plasma parameters such as the density and the plasma length. The Raman compression effect can set the stage for the wakefield self-compression effect to further shorten the pulse duration.

We would like to acknowledge Dr. A. Andrianov for valuable discussions on SPIDER measurements. This research has been supported by the DFG SFB/TR 18 and the GRK 1203 programs. S.A.S. and E.A.A. also acknowledge partial support from the RFBR Grant No. 12-02-33074, RF President Grant No. MK-5853.2013.2, and the Dynasty Foundation.

[1] D. Strickland and G. Mourou, Opt. Commun. **56**, 219 (1985).
[2] J. H. Sung *et al*., Opt. Lett. **35**, 3021 (2010).
[3] www.extreme-light-infrastructure.eu/; http://www.izest.polytechnique.edu/.
[4] V. M. Malkin, G. Shvets, and N. J. Fisch, Phys. Rev. Lett. **82**, 4448 (1999).
[5] F. Krausz and M. Ivanov, Rev. Mod. Phys. **81**, 163 (2009).
[6] K. Schmid *et al*., Phys. Rev. Lett. **102**, 124801 (2009).
[7] O. Chekhlov *et al*., Opt. Lett. **31**, 3665 (2006).
[8] V. V. Lozhkarev *et al*., Laser Phys. Lett. **4**, 421 (2007).
[9] D. Herrmann *et al*., Opt. Lett. **34**, 2459 (2009).
[10] S. A. Skobelev, A. V. Kim, and O. Willi, Phys. Rev. Lett. **108**, 123904 (2012).
[11] O. Shorokhov, A. Pukhov, and I. Kostyukov, Phys. Rev. Lett. **91**, 265002 (2003).
[12] C. Ren, B. J. Duda, R. G. Hemker, W. B. Mori, T. Katsouleas, T. M. Antonsen, and P. Mora, Phys. Rev. E **63**, 026411 (2001).
[13] M. Lontano and I. G. Murusidze, Opt. Express **11**, 248 (2003).
[14] D. F. Gordon, B. Hafizi, R. F. Hubbard, J. R. Penano, P. Sprangle, and A. Ting, Phys. Rev. Lett. **90**, 215001 (2003).
[15] L. A. Abramyan, A. G. Litvak, V. A. Mironov, and A. M. Sergeev, Sov. Phys. JETP **75**, 978 (1992).
[16] J. Faure, Y. Glinec, J. J. Santos, F. Ewald, J. P. Rousseau, S. Kiselev, A. Pukhov, T. Hosokai, and V. Malka, Phys. Rev. Lett. **95**, 205003 (2005).
[17] J. Schreiber, C. Bellei, S. P. D. Mangles, C. Kamperidis, S. Kneip, S. R. Nagel, C. A. J. Palmer, P. P. Rajeev, M. J. V. Streeter, and Z. Najmudin, Phys. Rev. Lett. **105**, 235003 (2010).
[18] L. Gallmann *et al*., Opt. Lett. **24**, 1314 (1999).
[19] A. S. Wyatt and I. A. Walmsley, Opt. Lett. **31**, 1914 (2006).
[20] C. E. Max, J. Arons, and A. B. Langdon, Phys. Rev. Lett. **33**, 209 (1974).
[21] S. F. Martins *et al*., Phys. Plasmas **17**, 056705 (2010)
[22] A. Pukhov and J. Meyer-ter-Vehn, Appl. Phys. B **74**, 355 (2002); W. Lu *et al*., Phys. Rev. ST **10**, 061301 (2007).
[23] M. Geissler, G. Tempea, A. Scrinzi, M. Schnurer, F. Krausz, and T. Brabec, Phys. Rev. Lett. **83**, 2930 (1999).
[24] P. Sprangle, E. Esarey, J. Krall, and G. Joyce, Phys. Rev. Lett. **69**, 2200 (1992).
[25] E. Esarey, C. B. Schroeder, and W. P. Leemans, Rev. Mod. Phys. **81**, 1229 (2009).